Available online at www.sciencedirect.com
SCIENCE DIRECT
Geochimica et Cosmochimica Acta 70 (2006) 504–515
Geochimica
www.elsevier.com/locate/gca

High-pressure phases in a shock-induced melt vein of the Tenham L6 chondrite: Constraints on shock pressure and duration

Zhidong Xie [a,*], Thomas G. Sharp [a], Paul S. DeCarli [b]

[a] *Geological Sciences Department, Arizona State University, Tempe, AZ 85287, USA*
[b] *SRI International, 333 Ravenswood Ave., Menlo Park, CA 94025, USA*

Received 31 March 2005; accepted in revised form 12 September 2005

Abstract

The microtexture and mineralogy of a 580-μm-wide melt vein in the Tenham L6 chondrite were investigated using field-emission scanning electron microscopy and transmission electron microscopy to better understand the shock conditions. The melt vein consists of a matrix of silicate plus metal-sulfide grains that crystallized from immiscible melts, and sub-rounded fragments of the host chondrite that have been entrained in the melt and transformed to polycrystalline high-pressure silicates. The melt-vein matrix contains two distinct textures and mineral assemblages corresponding to the vein edge and interior. The 30-μm-wide vein edge consists of vitrified silicate perovskite + ringwoodite + akimotoite + majorite with minor metal-sulfide. The 520-μm-wide vein interior consists of majorite + magnesiowüstite with irregular metal-sulfide blebs. Although these mineral assemblages are distinctly different, the pressure stabilities of both assemblages are consistent with crystallization from similar pressure conditions: the melt-vein edge crystallized at about 23–25 GPa and the vein interior crystallized at about 21–25 GPa. This relatively narrow pressure range suggests that the melt vein either crystallized at a constant equilibrium shock pressure of ~25 GPa or during a relatively slow pressure release. Using a finite element heat transfer program to model the thermal history of this melt vein during shock, we estimate that the time required to quench this 580-μm-wide vein was ~40 ms. Because the entire vein contains high-pressure minerals that crystallized from the melt, the shock-pressure duration was at least 40 ms. Using a synthetic Hugoniot for Tenham and assuming that the sample experienced a peak-shock pressure of 25 GPa near the impact site, we estimate that the Tenham parent body experienced an impact with collision velocity ~2 km/s. Based on a one-dimensional planar impact model, we estimate that the projectile size was >150 m in thickness.
© 2005 Elsevier Inc. All rights reserved.

1. Introduction

Tenham fell in 1879 near Tenham Station (25°44′S, 142°57′E) in South Gregory, Queensland, Australia (Spencer, 1937). Tenham is a famous highly shocked L6 chondrite that contains metastable high-pressure minerals in the melt veins, including ringwoodite, majorite, wadsleyite, magnesiowüstite, akimotoite, silicate-perovskite, and hollandite-structured plagioclase (Binns et al., 1969; Langenhorst et al., 1995; Madon and Poirier, 1983; Mori and Takeda, 1985; Price et al., 1979; Putnis and Price, 1979; Tomioka and Fujino, 1997; Tomioka et al., 2000). The presence of glassy plagioclase and polycrystalline ringwoodite in melt vein regions of Tenham indicates a shock stage of S6 (Xie and Sharp, 2000), which has been inferred to correspond to a pressure between ~45 and ~90 GPa (Stöffler et al., 1991). However, calibration of the shock pressures required to transform silicates to their high-pressure polymorphs is dependent on kinetics and therefore dependent on the P-T-t conditions of shock. Most of the high-pressure minerals found in Tenham are stable at pressures ranging from 14 to 27 GPa (Agee et al., 1995; Fei and Bertka, 1999; Gasparik, 1992; Irifune, 1993; Ito and Yamadah, 1982; Katsura and Ito, 1989; Kerschhofer et al., 1996; Ringwood, 1958; Trønnes, 2000) and have never been synthesized in shock recovery experiments. The crystallization of silicate melt during shock commonly produces minerals and assemblages that are stable at moderately high

* Corresponding author.
E-mail addresses: zhidong.xie@asu.edu (Z. Xie), tom.sharp@asu.edu (T.G. Sharp), paul.decarli@sri.com (P.S. DeCarli).

0016-7037/$ - see front matter © 2005 Elsevier Inc. All rights reserved.
doi:10.1016/j.gca.2005.09.003

pressures (14–27 GPa), suggesting that equilibrium shock pressure in chondrite parent bodies may be much less than those implied by calibration of shock stage S6.

The high-pressure phases in Tenham and other meteorites are invariably found within or adjacent to shock melt veins. These veins are actually sheets, ranging in thickness from ~1 μm to several mm, which appear vein-like in thin section. Petrographic evidence supports the view that the veins comprise material that was locally melted (Fredriksson et al., 1963) and then quenched by conduction to the surrounding cooler host rock (Langenhorst and Poirier, 2000; Leroux et al., 2000; Sharp et al., 2003). The melt veins commonly contain two distinct parageneses. One consists of polycrystalline grains produced by the solid-state transformation of host-rock fragments. Rounded grains of blue polycrystalline ringwoodite are easy to observe petrographically and provide one indictor of S6 shock grade (Stöffler et al., 1991). The other paragenesis consists of a matrix of silicate plus metal-sulfide grains that crystallized from immiscible silicate and sulfide melts. The resulting fine-grained crystals require high-resolution techniques for characterization and mineral identification (Chen et al., 1996). Close similarities in mineralogy, grain size, composition, and microstructure between the samples from static high-pressure melting experiments and the assemblages that crystallize from melt veins in highly shocked meteorites suggest that phase diagrams obtained from static high-pressure experiments can be used to constrain the conditions of melt-vein crystallization (Chen et al., 1996; Sharp et al., 2000). Recent studies of shock-induced melt veins show that melt-vein matrix assemblages provide constraints on crystallization conditions and shock pressure (Chen et al., 1996; Gillet et al., 2000; Langenhorst and Poirier, 2000; Sharp et al., 1997, 2001; Xie and Sharp, 2004; Xie et al., 2001, 2002). In addition, melt-vein assemblages have the added advantage of recording crystallization history as the melt vein cools from the edge to the center (Langenhorst and Poirier, 2000; Sharp et al., 2003). If melt-vein crystallization occurs at almost constant equilibrium shock pressure, the mineral assemblages will be consistent with crystallization at constant pressure. If melt-vein crystallization occurs during pressure release, the center of the melt vein, which crystallizes last, is likely to have minerals that are stable at pressures lower than those that crystallized at the melt-vein margin. The time scales of melt-vein crystallization can be estimated as a function of vein thickness through use of one-dimensional heat flow calculations (DeCarli et al., 2002a,b; Langenhorst and Poirier, 2000; Sharp et al., 2002).

This study is part of an ongoing investigation of shock-induced melt veins as indicators of crystallization conditions and focuses primarily on the melt-vein matrix. To test for changing pressure conditions during melt-vein crystallization, we mapped textural and mineralogical changes across a 580-μm wide vein. Transmission electron microscopy (TEM) was the primary tool for identifying the mineral assemblages of the melt-vein matrix. Mineralogy combined with the relevant phase-equilibrium data was used to constrain the crystallization pressure. The minimum duration of the shock pulse was estimated from the time required to cool the melt vein to below the solidus for similar melt compositions. Constraints on shock pressure, obtained from estimates of crystallization pressure, have been used to estimate a lower bound on the impact velocity. The estimate of minimum shock pressure duration establishes lower bounds on the sizes of the impacting body.

2. Methods

A 31.6 g piece of the Tenham L6 chondrite was obtained from the Center for Meteorite Studies at Arizona State University (ASU sample #647.6) and a 30 μm thin section was made for the study. The sample was investigated with a combination of optical petrography using transmitted and reflected light, scanning electron microscopy (SEM) with thermal and field-emission electron sources, and analytical transmission electron microscopy (ATEM), also using both thermal and field-emission electron sources.

Petrography and SEM were used to locate melt veins and melt pockets, to study the shock features of the host rock, and to identify large polycrystalline ringwoodite grains and large host rock fragments in the opaque melt veins. The textures of the melt veins and semi-quantitative chemical analysis of minerals in the melt veins were investigated using JEOL JSM-840 SEM and Hitachi S-4700 field-emission SEM instruments, both equipped with energy dispersive X-ray spectroscopy (EDS) systems.

Because the grain size of the minerals in the melt veins and pockets ranges from hundreds of nanometers to several micrometers, ATEM is an essential tool for their characterization. A 3 mm diameter sample disk containing a 580 μm wide vein was cored from the thin section and adhered to a copper TEM grid with a 1 mm diameter hole. The disk center was mechanically thinned to ~10 μm using a Gatan Dimple Grinder (model 656) and then ion milled using a Gatan Precision Ion Polishing System (PIPS). The specimen was thinned to electron transparency using Ar-ions accelerated to 5 keV and bombarding the sample surface at an incidence angle of 4–6°. ATEM data were recorded from the thin edges of ion-milled holes using JEOL JEM-2000FX and Philips CM200-FEG microscopes operated at 200 kV, both equipped with KEVEX EDS detectors and EmiSpec analytical systems for chemical analysis. The EDS detectors have ultrathin windows and can detect elements heavier than B. However, elements lighter than Na are subjected to strong absorption. Conventional TEM imaging techniques were employed to characterize the microtextures of the vein and the microstructures of the minerals. Mineral phases were identified on the basis of quantitative EDS and selected area electron diffraction (SAED).

EDS analyses were quantified using the ratio technique of Cliff and Lorimer (1975). K factors relative to Si for

the major elements, Mg, Fe, Ca, Al, and O, were determined from standards using the method of van Cappellen (1990). The standards included fayalite for Fe and O; San Carlos olivine for Mg, Fe, and O; Johnstown orthopyroxene for Mg, Fe, and O; and Hakone anorthite for Al, Ca, and O. Although oxygen data were collected and reported (Table 1), they were not used to correct for absorption effects or to calculate the formula. Calculations of mineral formulas were based on the number of oxygen anions in the formula and oxidation states of the cations. It was assumed that all Fe in silicates was Fe^{2+}.

Mineral assemblages in the melt vein matrix, characterized by TEM, were used, in combination with phase relation data, to constrain the crystallization pressure of the melt vein. Crystallization of the silicate melt during rapid quenching of a shock vein is likely to occur from a supercooled liquid (Langenhorst and Poirier, 2000), which can result in metastable crystallization of subliquidus and even subsolidus phases. Although supercooling can result in disequilibrium assemblages, the high pressure minerals that crystallize, combined with their pressure stabilities, still provide constraints on the pressure of crystallization. The approach is not to assume chemical equilibrium and determine exact crystallization pressure and temperature from phase-equilibrium data, but rather to constrain the crystallization pressure from the overall pressure stabilities of the minerals that crystallized from the melt.

The calculation of minimum quench duration for a vein was performed using a finite element heat transfer program (FEHT) (Klein et al., 2002). The calculation assumes an initial vein temperature of 2700 K, a density of 4310 kg/m^3 at a pressure of 25 GPa, and a conductivity of 10 W/mK (see Section 4.3). A synthetic Hugoniot was constructed for Tenham from the properties of the mineral constituents (Ahrens and Johnson, 1995b) and used (Walsh and Christian, 1955) to estimate post-shock and shock temperatures of 620 and 660 K, respectively, as well as density and other parameters for a shock pressure of 25 GPa. Crystallization of the melt vein starts after the melt-vein temperature drops below the liquidus, which is obtained from published phase diagrams. The results of the calculation are temperature–time profiles for the vein center and vein edge. The lag time between crystallization of vein edge and vein center provides a minimum quench time of the vein.

3. Results

3.1. Overview of shock features

The major minerals in Tenham include olivine, orthopyroxene, and plagioclase, with minor amounts of iron–nickel alloy, troilite, and other minor minerals. Olivine and pyroxene show pervasive fracturing. Most pyroxenes show strong mosaicism, whereas olivines range from having strong mosaicism to sharp extinction. Most olivine grains that occur adjacent to melt veins show a yellow to yellow-brown staining, which is inferred to correspond to

Table 1
TEM EDS analysis of high-pressure phases in melt vein

	ak(3)	pv(7)	m-maj(7)	s-maj(5)	m-rw(6)	p-rw(4)	mw(3)	glass(4)
At %								
O*	60.25	57.90	58.70	59.05	56.96	55.77	53.60	64.21
Na		1.56	0.65	0.12				0.09
Mg	17.57	16.69	15.56	16.36	18.67	21.81	31.73	15.08
Al	0.90	1.08	1.74	0.30	0.22			0.79
Si	18.87	18.87	19.03	20.26	14.09	14.61		14.74
Ca	0.08	0.68	1.32	0.22	0.03			1.01
Fe	2.33	3.15	3.01	3.67	10.00	7.82	14.25	3.98
Cr	0.02	0.02		0.01	0.05		0.42	0.03
K								
Mn		0.05						0.08
Formula unit								
O	3	3	3	3	4	4	1	
Na		0.08	0.03	0.01				
Mg	0.89	0.82	0.77	0.80	1.30	1.48	0.68	
Al	0.05	0.05	0.09	0.01	0.02			
Si	0.96	0.93	0.94	0.99	0.98	0.99		
Ca	0.00	0.03	0.06	0.01	0.00			
Fe	0.12	0.16	0.15	0.18	0.70	0.53	0.31	
Cr	0.00	0.00		0.00	0.00		0.01	
K								
Mn		0.00						

Note. O* at% is measured data. However, these oxygen data were not used to calculate the mineral formulas. Mineral formulas calculated from the cation measurements based on the assumption of stoichiometry and the assumption that all Fe are Fe^{2+}. Number in brackets is the number of EDS spectra averaged. ak, akimotoite; pv, perovskite; m-maj, matrix majorite; s-maj, low-Al-Ca majorite; m-rw, matrix ringwoodite; p-rw, polycrystalline ringwoodite; mw, magnesiowüstite; and glass, melt-vein silicate glass.

recrystallization (Stöffler et al., 1991). All plagioclase grains have been transformed to optically isotropic maskelynite or normal glass and throughout the thin section many grains show flow textures that suggest melting. We did not find remnants of plagioclase in maskelynite, which have been reported to occur in areas remote from melt veins (Bennett and McSween, 1996; Binns, 1970). Abundant ringwoodite in the melt veins, glassy plagioclase in the host rock, and recrystallization of olivine indicate a shock stage of S6 according to the shock classification of Stöffler et al. (1991).

The thin section contains a dense network of black veins running randomly throughout the sample, with width ranging from ~0.005 mm up to 1.5 mm. We have determined the mineral assemblages that have crystallized from veins of various widths and found that the assemblages vary greatly. The thinnest vein that we observed was 5 μm wide and contains predominantly silicate glass and metal-sulfide droplets. This suggests a very rapid quench, which is expected for the thinnest melt veins. A 580 μm wide melt vein, which encloses small, rounded, multi-phase fragments of host rock (Figs. 1A and B), is the main focus of this study. Most of these fragments are small (less than 100 μm) blue grains of polycrystalline ringwoodite, as previously described (Binns et al., 1969). Other entrained fragments include pyroxene or their high-pressure polymorphs and a whole chondrule (Figs. 1A and B). The abundance of fragments suggests that this vein did not form by injection into a fracture, but rather formed in situ by shearing or collapsing around cracks and pores.

The black vein matrix, which accounts for most of the material in the 580 μm vein, consists of micron-sized, equant, isotropic crystals, and droplets or blebs of metal-sulfide. Equant isotropic crystals in the vein matrix have been identified as majorite (Langenhorst et al., 1995; Price et al., 1979), a high-pressure garnet of $(Na,Ca,Mg,Fe)_3(Mg,Fe,Al,Si)_2Si_3O_{12}$ with up to 25% of Si^{4+} in octahedral coordination. Metals and sulfides present in the vein include kamacite, taenite, and troilite (Price et al., 1979). Our FESEM and TEM results show that the mineralogy and micro-texture of the matrix of the vein edge differ from those of the vein interior.

3.2. Melt-vein edge

The 580 μm melt vein contains a distinct vein-edge region that is ~30 μm wide and consists of a mixture of equant and irregular-shaped grains with few rounded metal-sulfide droplets (Figs. 2A and B). TEM imaging and electron diffraction show that the equant grains are amorphous silicate (Fig. 2C). The grain sizes range from 1 to 3 μm in diameter. Quantitative EDS analysis (Table 1) gives the composition as $Na_{0.08}Ca_{0.03}Mg_{0.82}Fe_{0.16}Al_{0.05}Si_{0.93}O_3$, which is similar to the composition of matrix majorite and consistent with the composition of silicate-perovskite that would crystallize from a chondritic melt (Sharp et al., 1997). The morphology and composition are similar to those of the vitrified silicate-perovskite in the Acfer 040 chondrite (Sharp et al., 1997), in Suizou meteorite (Chen et al., 2004b), and in the Zagami achondrite (Langenhorst and Poirier, 2000). Unlike the previously reported silicate-perovskite in Tenham (Tomioka and Fujino, 1997), which formed by a solid-state transformation from enstatite, these vitrified grains of silicate-perovskite are part of the melt-vein edge matrix and therefore crystallized from the silicate melt at high pressure, like those reported in Acfer 040 (Sharp et al., 1997). Based on the uniform contrast observed in BSE images (Fig. 2B), these grains were homogeneous, and probably amorphous, prior to TEM sample preparation. The materials surrounding the vertrified silicate-perovskite include ringwoodite, majorite, and other unidentified nanocrystalline phases.

Most irregular crystals in the vein edge are ringwoodite (Fig. 2B). The ringwoodite grains can be either equant, somewhat elongated, or irregular-shaped, ranging in size from hundreds of nm to 1 μm. The grains have high densities of stacking faults on {110}, which are characteristic features of ringwoodite in meteorites (Chen et al., 1996;

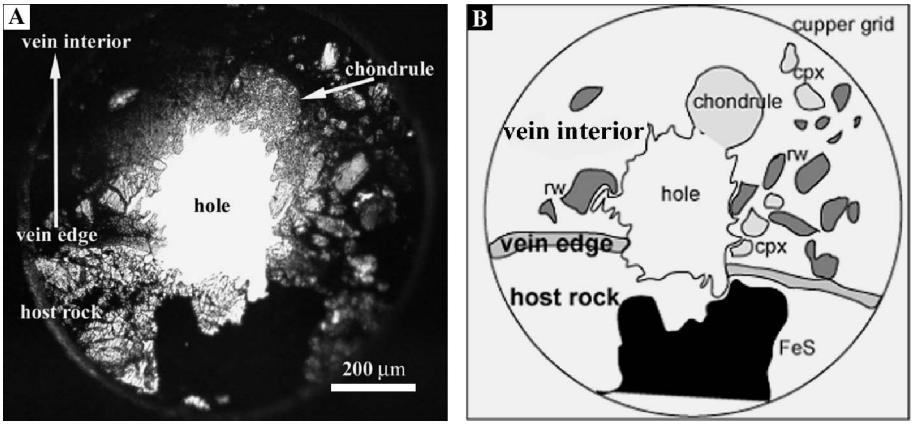

Fig. 1. (A) Petrographic image of a thinned TEM sample of Tenham with a hole in the center. (B) Sketch of the TEM sample showing the vein edge and interior with fragments of host rock, including ringwoodite (rw), clinopyroxene (cpx), and a chondrule.

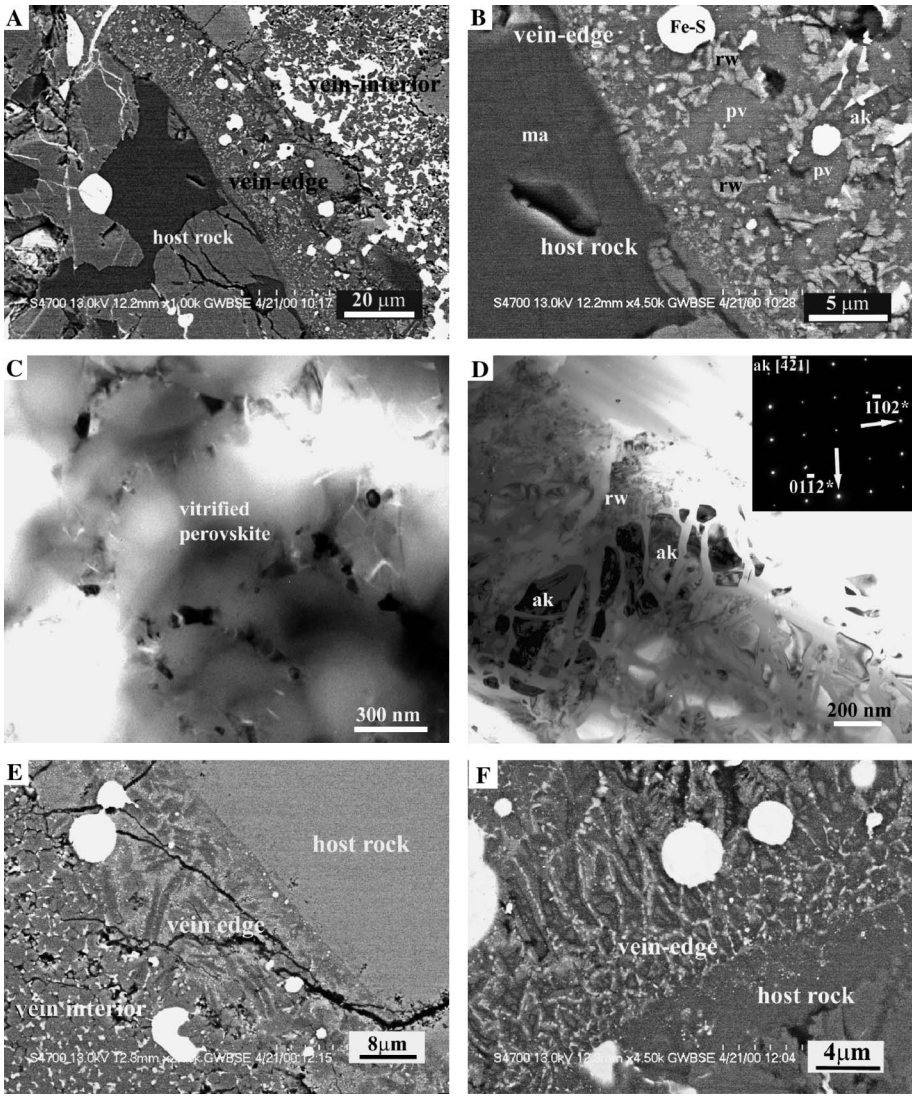

Fig. 2. (A) FESEM image showing the textures of the melt-vein edge and vein interior. Note that the vein interior has a higher abundance of metal-sulfide. (B) Higher magnification FESEM image of the vein-edge region showing equant grains of vitrified perovskite (pv), irregular-shaped ringwoodite (rw), elongated crystal of akimotoite (ak), and round metal-sulfide droplets (Fe–S). The host rock touching the vein in this image is maskelynite (ma). (C) Bright-field TEM image showing equant grains of vitrified perovskite surrounded by smaller crystals in the melt-vein edge of Tenham. Most of these small crystals are ringwoodite. (D) Bright-field TEM image of partially vitrified akimotoite (ak) with ringwoodite (rw) in a silicate glass matrix in the melt-vein edge of Tenham. The electron diffraction pattern shows the [-4-21] zone axis of the strongly diffracting dark akimotoite crystals in the center of the image. (E) FESEM image of melt-vein edge opposite to that shown in A and B. This image shows two distinct textures: the vein interior with equant grains and vein edge with skeletal quench texture. (F) FESEM image of a vein-edge region showing a similar skeletal quench texture on the opposite side of the melt vein.

Madon and Poirier, 1983; Putnis and Price, 1979; Sharp et al., 1997). EDS analysis shows that the ringwoodite with a composition of $Mg_{1.3}Fe_{0.7}Al_{0.02}Si_{0.98}O_4$ contains more Al_2O_3 and FeO than the host olivine (Fa_{26}) and the polycrystalline ringwoodite ($Mg_{1.48}Fe_{0.53}Si_{0.99}O_4$) (Table 1), consistent with its crystallization from the silicate melt.

Akimotoite ($Mg_{0.89}Fe_{0.12}Al_{0.05}Si_{0.96}O_3$), which occurs along with ringwoodite, forms long crystals up to 5 μm in length that are partially vitrified and surrounded by silicate glass (Fig. 2D). Electron diffraction patterns from these grains are consistent with the ilmenite structure (Fig. 2D). Akimotoite found here is different from the previously reported akimotoite in Tenham (Tomioka and Fujino, 1997), which formed by solid-state transformation of enstatite. Based on the intimate association with ringwoodite that crystallized from the melt and the higher Al_2O_3 content than that of host enstatite, the akimotoite described here, like that found in Acfer 040 (Sharp et al., 1997) and in Umbarger (Xie and Sharp, 2004), crystallized from the silicate melt.

FESEM imaging shows a skeletal inter-cumulus quench texture on the opposite edge of the melt vein (Figs. 2E and F). This typical quench texture is similar to that seen in static state high-pressure experiments on peridotites (Zhang and Herzberg, 1994), which is characteristic of rapid quench.

3.3. Melt-vein interior

The 520 μm wide melt-vein interior consists of equant silicate crystals, and high atomic number phases, which consist of irregular-shaped oxides and metal-sulfide blebs (Figs. 3A–C). The equant grains are majorite garnet, consistent with previous studies of Tenham (Binns, 1970; Langenhorst et al., 1995; Madon and Poirier, 1983; Mori and Takeda, 1985; Price et al., 1979; Putnis and Price, 1979). Majorite occurs as crystals ranging in size from 2 to 5 μm (Figs. 3B and C). EDS analysis of majorite gives the composition as $Na_{0.12}Ca_{0.24}Mg_{3.08}Fe_{0.60}Al_{0.36}Si_{3.76}O_{12}$, which is enriched in Al_2O_3, CaO, and Na_2O compared to the host enstatite composition, or low-Al-Ca majorite ($Na_{0.04}Ca_{0.04}Mg_{3.20}Fe_{0.72}Al_{0.04}Si_{3.96}O_{12}$), which is formed by solid-state transformation of enstatite (Table 1). The occurrence in the melt-vein matrix and the relatively high Al_2O_3, CaO, and Na_2O values are consistent with the matrix garnets crystallizing from the shock-induced chondritic silicate melt. An interstitial silicate glass occurs between the majorite crystals (Fig. 3D), suggesting that crystallization of the melt vein was incomplete, leaving a small amount of residual interstitial glass. The interstitial glass has a composition rich in MgO and SiO_2 (Table 1).

Irregular crystals of magnesiowüstite occur between the majorite grains (Fig. 3D). Magnesiowüstite was first reported in Tenham as inclusions in Al-bearing majorite (Mori and Takeda, 1985). The occurrence of magnesiowüstite between majorites in the quenched silicate melt indicates that it crystallized along with the majorite, as has been reported in Sixiangkou (Chen et al., 1996) and RC106 (Aramovich et al., 2003). EDS analysis of these magnesiowüstite grains gives the composition as $(Mg_{0.68}Fe_{0.31}Cr_{.0.01})O$ (Table 1). TEM imaging and diffraction also show that tiny magnetite crystallites (from 3 to 20 nm in size) are coherently intergrown throughout the magnesiowüstite (Fig. 3D), similar to those reported by Chen et al. (1996). The presence of magnetite indicates either a breakdown of magnesiowüstite to magnetite plus ferropericlase or exsolution of magnetite from nonstoichiometric magnesiowüstite that was rich in ferric iron. In either case, the removal of magnetite from the magnesiowüstite would have made the remaining magnesiowüstite richer in periclase.

The melt-vein interior shows a distinctly different texture from those of the vein edges. Vein edges have more irregular silicate crystal forms and rounded metal-troilite droplets, whereas the vein interior has more euhedral and equant silicate crystal forms and irregular-shaped metal-troilite blebs. The matrix of the vein interior has a liquidus crystallization texture similar to those from the static high-pressure experiments (Agee et al., 1995; Zhang and Herzberg, 1994). The transition from vein edge to vein interior in some location is marked by an abrupt change in the amount of metal-sulfide melt in Fig. 2A. However, images of the opposite vein edge (Figs. 2E and F) do not show an abrupt compositional change.

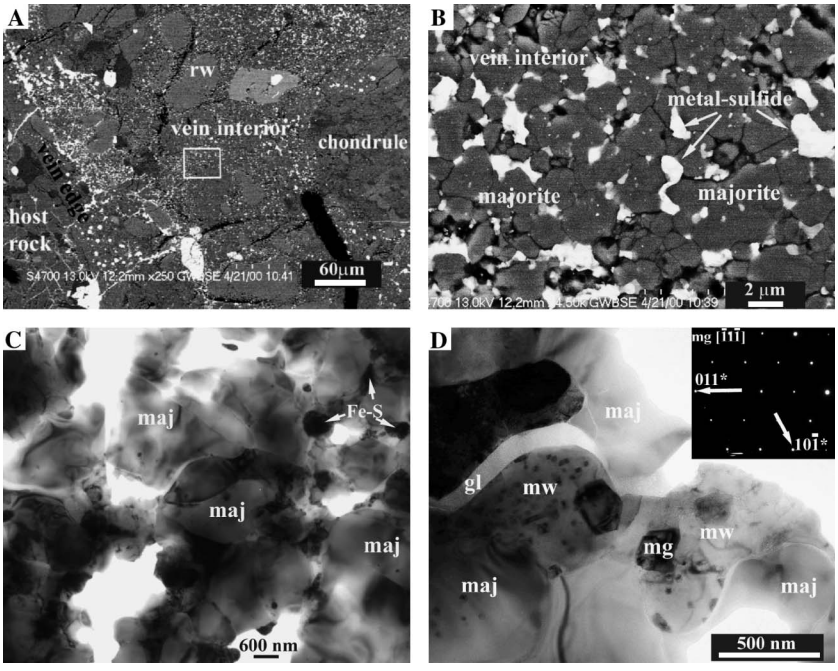

Fig. 3. (A) Low magnification FESEM image of the melt vein showing narrow vein-edge and wide vein-interior regions. White blebs correspond to Fe–Ni metal and Fe-sulfide, whereas large gray grains are entrained ringwoodite (rw). (B) High magnification FESEM image of the vein interior region, from the rectangular box of Fig. 3A, showing equant majorite crystals and irregular oxide grains and metal-sulfide blebs. (C) Bright-field TEM image of vein interior showing equant majorite (maj) and dark contrast metal-sulfide (Fe–S) grains. (D) Bright-field TEM image of the vein interior showing equant majorite (maj), interstitial glass (gl), and magnesiowüstite (mw) intergrown with magnetite (mg). The SAED pattern shows the [-11-1] zone axis of dark magnetite in the image center.

4. Discussion

4.1. Crystallization pressure

The majorite + magnesiowüstite assemblage in the Tenham melt vein also occurs in melt veins from other highly shocked chondrites such as Sixiangkou (Chen et al., 1996) and in RC106 (Aramovich et al., 2003). In addition, this assemblage in the melt vein is strikingly similar in mineralogy, grain size, composition, and texture to those of the assemblages produced in melting experiments on KLB-1 peridotite (Zhang and Herzberg, 1994) and on the Allende CV3 chondrite (Agee et al., 1995). Like the products from static high-pressure melting experiments, the melt-vein interior of Tenham has equant majorite crystals plus interstitial magnesiowüstite and residual glass. The majorites in Tenham, like those from static experiments on Allende (Agee et al., 1995), range from 2 to 5 μm in size, while those from experiments on KLB-1 periodotite are 10–20 μm (Zhang and Herzberg, 1994).

The similarities between the melt-vein assemblage and those from static high-pressure experiments suggest that phase diagrams obtained from static high-pressure experiments can be used to constrain the conditions of melt-vein crystallization (Chen et al., 1996). In doing so, we do not assume that the melt-vein assemblage represents chemical equilibrium, but instead use the pressure stabilities of the high-pressure minerals to constrain the pressure of melt-vein crystallization. One problem in this approach is that there are little experimental data for high-pressure melting of L-chondrite compositions such as that of Tenham, A recent paper by Chen et al. (2004b) presents results of seven melting experiments on the L-chondrite M'bale, but these data correspond to low levels of melting and there are insufficient data to construct a phase diagram. The most complete experimental data available are for the Allende CV carbonaceous chondrite (Agee et al., 1995) and for the Kilburn-Hole Peridotite KLB-1 (Zhang and Herzberg, 1994). The phase diagrams for these two compositions differ significantly in terms of liquidus temperatures and assemblages, reflecting the difference in chemical composition between a CV chondrite and a peridotite. Allende has about 27 wt% FeO in the silicate and is richer in moderately volatile elements, which results in a melting temperature lower than that of KLB-1, which has 9 wt% FeO. In both compositions, majorite garnet is the liquidus phase between about 15 and 23–25 GPa, but in KLB-1, magnesiowüstite also has a broad range of stability (17–23 GPa) near the liquidus (Fig. 4), which is significantly lower than the 23–27 GPa stability range of magnesiowüstite in Allende. In M'bale, which has an FeO content (14.1 wt%) very similar to that of Tenham 14.4 wt% FeO in melted areas (Leroux et al., 2000), magnesiowüstite occurs between 21 and 25 GPa. Therefore, the majorite + magnesiowüstite assemblage in Tenham probably corresponds to a crystallization pressure range that is intermediate between that of KLB-1 (17–23 GPa) and Allende (23–27 GPa) and very similar to

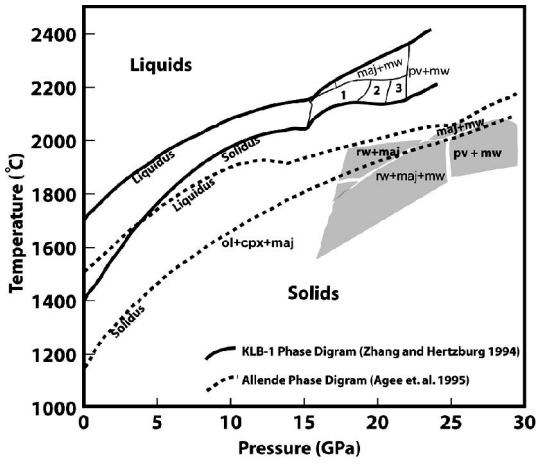

Fig. 4. Combined and simplified versions of the Allende phase diagram (Agee et al., 1995) and KLB-1 phase diagram (Zhang and Herzberg, 1994). rw, ringwoodite; maj, majorite; mw, magnesiowüstite; pv, perovskite; 1, liquid + majorite + wadsleyite; 2, liquid + majorite + wadsleyite + magnesiowüstite; 3, liquid + majorite + magnesiowüstite + ringwoodite + Ca-perovskite.

that of M'Bale (21–25 GPa). Because Tenham is closer in FeO content to KLB-1 than it is to Allende, the liquidus temperature for Tenham over this pressure range is likely to be closer to the 2200–2400 °C range of KLB-1 than to the 2000–2100 °C range of Allende (Fig. 4).

The crystallization pressure of the melt-vein edge region is more complicated because the silicate-perovskite + akimotoite + ringwoodite + majorite assemblage in the edge region is not predicted by any of the phase diagrams. Akimotoite is a subsolidus phase that is stable with ringwoodite at 18–25 GPa in the enstatite–forsterite system and is metastable relative to majorite at liquidus temperatures (Gasparik, 1992). Akimotoite is likely to be a subsolidus phase in an L-chondrite at high pressure, which is consistent with the data from M'Bale (Chen et al., 2004a). Akimotoite probably represents metastable crystallization from a supercooled silicate liquid during rapid quench. The equant glassy grains that occur in the melt-vein edge regions are inferred to be silicate-perovskite that crystallized at high pressure and vitrified after pressure release as a result of post-shock temperatures above the thermal stability of silicate-perovskite. The low pressure stability limit of silicate-perovskite is 25 GPa in Allende (Agee et al., 1995), 22 GPa in KLB-1 (Zhang and Herzberg, 1994) (Fig. 4), and 23 GPa in M'Bale (Chen et al., 2004a). Therefore, the crystallization pressure for the melt-vein edge is about 23–25 GPa.

The difference in texture and mineralogy between the melt-vein interior and edge may be the result of a higher quench rate at the vein edge. Based on our thermal modeling of melt-vein quench (see Section 4.3), the vein region within ~30 μm of the edge solidified is less than 30 μs, which is three orders of magnitude less than the 30 ms solidification time for the center of the vein. This is consistent with the observation that irregular crystals, skelatal

crystals, and dendritic textures occur in the rapidly quenched vein edge, while equant majorite grains occur in the vein interior.

4.2. Constraints on shock pressure from crystallization pressure

The response of a heterogeneous material to shock compression is extremely complex when viewed on a nanosecond time scale and on a μm distance scale. The shock front is chaotic, with order-of-magnitude differences in initial pressure due to shock wave interactions among grains of different shock impedance and to jetting around cracks and pores. The consequences of this pressure heterogeneity are reflected in localized temperature extremes, which have long been apparent in microscopic studies of shocked samples (Bischoff and Stöffler, 1992; DeCarli, 1979; Kieffer, 1971; Kieffer et al., 1976). It has recently become possible to computationally model the evolution of the chaotic shock front into the steady shock front predicted by continuum theory (Baer, 2000). These calculations predict that shock interactions around a pore can produce a transient (nanosecond duration) pressure excursion in a mm-size region that is more than 10 times the continuum pressure. These calculations are essentially validated by numerous microscopic studies, including those cited above. Adiabatic shear or localized deformation can also produce localized temperature extremes without a requirement for localized pressure differences (Nesterenko, 2001; Zener and Hollomon, 1944).

The term "peak pressure," as it is used by most shock-wave specialists, refers to the continuum pressure. If two Tenham-like bodies collide at a relative velocity of 2.1 km/s, the continuum pressure at the point of impact will be ~25 GPa. Assuming a mm grain size, the initial chaotic distribution of pressures, spanning the range from ~15 to >100 GPa, will equilibrate to ~25 GPa within <1 μs. The continuum pressure is occasionally referred to as the "equilibrium peak pressure." The word "equilibrium" should be used with caution; thermodynamic equilibrium is not implied, and the chaotic distribution of initial temperatures equilibrates much more slowly than the pressure heterogeneity, as shown in Section 4.3.

The key to using crystallization pressure of the melt-vein minerals to infer the shock pressure is to understand the temporal relationship between melt-vein crystallization and pressure release (Sharp et al., 2001). The key question is: did crystallization occur at constant (or slowly decreasing) peak pressure or did crystallization occur during a rapid decrease from much higher pressures inferred for shock stage S6 (Stöffler et al., 1991). If crystallization occurred during a large pressure release, we should see a difference in mineralogy between the vein edge and the vein center. If crystallization occurred at constant pressure or during a slow release of pressure, we should see mineral assemblages of similar pressure stabilities throughout a given melt vein. For Tenham, the constant mineral assemblage across the 520 μm vein interior (Fig. 3A) indicates a crystallization pressure range of ~21–25 GPa, which is consistent with the ~23–~25 GPa pressure inferred from mineral assemblages of the 30 μm vein edge (Fig. 2A). It is possible that the melt-vein edges crystallized at somewhat higher pressure than that of the vein interior, but there is no evidence of a large pressure decrease during the crystallization of the 520 μm thick melt vein. The situation is complicated by the fact that the vein-edge assemblages and textures are variable along the vein. The pressure constraints from the melt-vein edge and the melt-vein interior assemblage overlap and suggest that crystallization occurred at about 25 GPa and possibly during a modest pressure release from ~25 to ~21 GPa.

The shock pressure indicated by melt-vein crystallization is much lower than the shock pressures calibrated for S6 shock stage (45–90 GPa) features that occur adjacent to the melt vein (Stöffler et al., 1991). However, a crystallization pressure of ~25 GPa is not greatly different than that which one would estimate for S4 shock features that occur in the host rock away from melt veins. Based on planar deformation features (PDFs) in plagioclase and weak mosaicism in olivine in Tenham, a shock stage S4–S5 (25–45 GPa) was determined by Langenhorst et al. (1995). In addition, the unaltered plagioclase, which was reported to remain only in areas remote from the vein (Bennett and McSween, 1996; Binns, 1970), indicates an S4 shock stage (Bennett and McSween, 1996), which has a pressure range from 15–20 to 30–35 GPa. The pressure constraints provided by the high-pressure minerals in melt veins in this study are consistent with the pressure range attributed to the S4 shock stage, but not with S6 pressures. This consistency suggests that S6 features, which only occur in or adjacent to melt veins (Stöffler et al., 1991), can form at moderate shock pressures if temperatures are high enough to overcome the kinetic barriers for transformation effects.

4.3. Pressure-pulse duration

The temperature difference between the melt vein and host rock, which can be very high, determines the rate at which the melt vein quenches (Langenhorst and Poirier, 2000; Sharp et al., 2002; Sharp et al., 2003). Quenching begins as soon as the vein forms, independent of the pressure-pulse duration. The initial temperature of the melt vein must be greater than the solidus at shock pressure and is therefore at least 2300–2500 K at 25 GPa. It has previously been argued that the temperature decrease caused by adiabatic decompression is small compared to that caused by thermal conduction (DeCarli et al., 2002a,b; Langenhorst and Poirier, 2000; Sharp et al., 2003). Assuming an initial melt-vein temperature of 2700 K, the temperature T_f on release from 25 GPa to 1 atm. can be calculated from the approximate expression $T_f = 2700 \times e^{\Gamma(V_o - V)}$, where Γ is the Grüneisen parameter, and V_o and V are initial and final specific volumes of $0.2275\ cm^3\ g^{-1}$ and $0.2727\ cm^3\ g^{-1}$,

respectively (Walsh and Christian, 1955). For $\Gamma = 1.5$, Tf = 2523 K. The adiabatic temperature decrease of 173 °C is much smaller than the temperature difference between the melt vein and host rock, which is about 2000 °C at 25 GPa. Therefore, we can use thermal conduction to model the cooling histories of various points within and outside of a melt vein.

The calculation of minimum quench time was performed using a finite-element heat-transfer program (FEHT) (Klein et al., 2002). The input parameters include density at pressure, thermal conductivity, heat capacity as a function of temperature, initial host-rock shock temperature at pressure, and initial melt-vein temperature. Quantitative petrographic analysis of thin sections was used to measure the volume percentage of each major mineral in the Tenham meteorite. A synthetic Hugoniot for the meteorite was constructed from available mineral Hugoniot data (Ahrens and Johnson, 1995a,b) by addition of the volumes of each mineral constituent at pressure (DeCarli et al., 2004). From this Hugoniot, the calculated density of the bulk rock at 25 GPa is 4310 kg/m^3. A synthetic heat capacity table was constructed from C_P vs T data and heat of fusion data for the mineral constituents. However, we do not know the initial (pre-shock) porosity of the Tenham matrix. We therefore assume two possible cases, zero porosity and 7% porosity, in the form of homogeneously distributed small pores. We present these calculations to illustrate the effect of porosity.

The post-shock temperature calculation was based on the assumption that the meteorite was shocked to peak pressure via a single shock and that the release adiabat could be approximated by the zero-porosity Hugoniot. The waste heat, which is the area enclosed by the Rayleigh line and the release adiabat, ranges from ~85 J/g for the initially non-porous material to ~320 J/g for the 7% porous material. Equivalent post-shock temperatures range from ~400 to ~620 K. The corresponding shock temperature range at 25 GPa, calculated from the adiabatic temperature increase ($T_f = T_0 \times e^{\Gamma(V_o - V)}$), is 430–660 K. The initial matrix temperature was assumed to be 660 K, to allow for possible deformational heating not included in our simple calculation of shock temperature. We ignore the fact that the more compressible minerals, plagiaclase and troilite, will have shock temperatures much higher than those of pryoxene and olivine. We simply assume that the matrix is a homogeneous material having a homogeneous initial temperature.

A large uncertainty in the calculation is the high-pressure thermal conductivity, which is predicted to be in the range of 3–10 W/mK (van der Berg et al., 2001). The upper bound conductivity of 10 W/mK was used for the calculation to get the smallest and most conservative quench time. Another uncertainty in the calculation is the melt-vein temperature, which was based on the available phase diagrams. There are significant differences in the melting temperatures between the KLB-1 and the Allende phase diagrams. The solidus and liquidus temperatures in the Allende system are 2250 and 2310 K at 25 GPa, whereas in the KLB-1 system they are 2400 and 2630 K at 25 GPa, respectively (Fig. 4). Solidification occurs over a much higher temperature range for a melt of KLB-1 composition. Because heat conduction is proportional to the temperature difference between melt and matrix, the solidification time is expected to be shorter for the KLB-1 composition than for Allende. The high-pressure solidification time of a Tenham melt, intermediate in composition between Allende and KLB-1, should be bracketed by the solidification behaviors of KLB-1 and Allende. We therefore performed two sets of calculations as shown in Fig. 5. The solidification of the melt vein starts at the vein edge when the temperature there drops below the liquidus. Crystallization and solidification of the melt vein are complete when the temperature of the melt-vein center drops below the solidus, which is 2250 K at 25 GPa for Allende (Agee et al., 1995) and 2400 K for KLB-1 (Zhang and Herzberg, 1994). The initial melt-vein temperature was assumed to be 2700 K, which is somewhat higher than the liquidus temperature for KLB-1 at 25 GPa.

From the thermal model we calculate temperature vs. time profiles (Fig. 5) for the vein center (0.29 mm to vein wall), vein edge (0.02 mm inside the vein margin), the host rock near the vein (0.04 mm outside the vein), and the host rock 4 mm outside the vein. We calculate the total time required for the melt-vein to cool through the solidus temperature by taking the time difference between when the vein edge passes through the solidus and when the vein center passes through the solidus. Based on Allende data, we get a quench time of approximately 47 ms for the 580-μm-wide vein in Tenham (Fig. 5), whereas using the KLB-1 data we get a quench time of 33 ms. The average of these two values is ~40 ms for the 580-μm-wide vein. However, Tenham has many veins that contain high-pressure minerals and are wider than 580 μm and therefore required longer quench

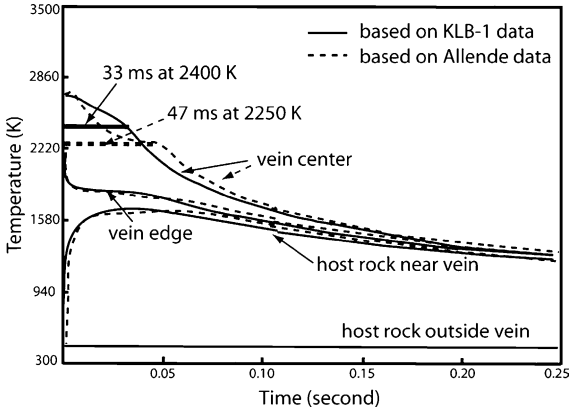

Fig. 5. Temperature vs. time profiles for the vein center, vein edge, and host rock for the 0.58-mm-wide vein in Tenham based on KLB-1 data (solid line) and Allende data (dotted line). The quench duration is the lag time between crystallization of vein edge and vein center, which is ~33 ms based on Allende data and ~47 ms based on KLB-1 data. The profiles for the vein center and vein edge correspond to 0.29 and 0.02 mm inside the vein-host interface, whereas the profiles of the host correspond to 0.04 and 4.0 mm outside the vein-host interface.

times. Because the entire 580-μm-wide vein contains high-pressure minerals that crystallized from the melt, the duration of shock pressure (above ~17 GPa) was at least 40 ms, and probably much longer, so that the vein could cool to a temperature that would permit survival of metastable high-pressure phases such as akimotoite. Ito and Navrotsky (1985) showed that $MgSiO_3$-akimotoite decomposes at 973 K at one atmosphere. Our cooling calculations indicate that ~0.5 s is required for the melt vein to cool below 973 K. This 0.5 s estimate is in general agreement with that of Beck et al. (2005), who used elemental diffusion in Tenham high-pressure phases to estimate a shock-pressure duration of ~1 s.

4.4. Calculation of impact conditions

The eventual goal for this study is to provide insight into the impact events that have affected chondrite parent bodies in the solar system. If we can infer the shock pressure and shock duration, we can estimate constraints on the relative velocity and sizes of the impacting bodies responsible for the effects observed in the meteorite.

For Tenham, we have used the melt-vein mineralogy to estimate a maximum shock pressure of 25 GPa. We have calculated a synthetic Hugoniot for Tenham by addition of the volumes of the constituents at pressure (Ahrens and Johnson, 1995a,b). The synthetic Hugoniot is a series of spreadsheet calculations based on the Hugoniot equations (see Sharp and DeCarli, 2006, for a detailed description)

$$U_p^2 = (P - P_o)(V_o - V),$$
$$U_s^2 = V_o^2(P - P_o)/(V_o - V),$$
$$E - E_o = (1/2)(P + P_o)(V_o - V),$$

where U_p and U_s are the particle and shock velocities, P_o and V_o are the initial pressure and volume, and E_o is the initial internal energy. To solve these equations for the constituent minerals of Tenham, we use the equation of state data from Ahrens and Johnson (1995a,b) relating the shock and particle velocities as

$$U_s = C_o + sU_p$$

From the synthetic Hugoniot, one can calculate the bulk shock velocity (U_s), particle velocity (U_p), and density (ρ) for Tenham as a function of pressure. At 25 GPa, the particle velocity for Tenham is 1.0 km/s. Assuming an impact between two Tenham-like bodies, the impact velocity is approximately twice the particle velocity (Walsh and Christian, 1955) or ~2 km/s. This impact velocity seems low in comparison with the average orbital velocities in the asteroid belt of ~25 km/s (Christiansen and Hamblin, 1995). However, calculations of the probability distribution of asteroid-asteroid collision velocities indicate a broad peak over the range of 2–7 km/s with a mean of 5.29 km/s (Bottke et al., 1994). One therefore cannot rule out the possibility that the shock effects in Tenham were caused by a 2 km/s collision. Alternatively, we can assume a higher collision velocity of 5 km/s. In this case, the peak shock pressure at the point of impact would be ~65 GPa. The material that would become the Tenham meteorite would have to be well below the surface of its parent body, to permit attenuation of the shock to a slowly decaying wave with a peak of about 25 GPa.

The minimum high-pressure duration of ~40 ms provides a basis for estimating the minimum sizes of the impacting bodies. For a simplified calculation, we assume that the impacting bodies are in the form of disks. The point of maximum shock duration will be on the impact surface at the center of the disk. If one assumes a collision between a small spherical asteroid and a much larger diameter body, one must resort to the use of a 2D wave propagation code to calculate the pressure-time history at the point of impact. For the simple one-dimensional planar impact model, the size of the projectile can be approximated using a simple equation: $\Delta t = d/U_s + d'/U_r$, where Δt is the duration of the peak pressure pulse ($\Delta t = 40$ ms for the Tenham case), d is the unknown thickness of projectile, and d' is the thickness of the projectile after compression. The compressed thickness d' is approximated as $d' = d(V'/V_0)$ for a one dimension model, where V_0 is the initial volume of the material and V' is the volume of the material at 25 GPa shock pressure. From the synthetic Hugoniot, V'/V_0 is 0.834. Based on the Hugoniot equation $U_s = (1/\rho_0)[(P - P_0)(V_0 - V)]^{1/2}$, the shock velocity at 25 GPa is 6.4 km/s. The release wave velocity is $U_r = [(K + 4\,\mu/3)/\rho]^{1/2}$, where K is the bulk modulus, which is the slope of the release adiabat at pressure, μ is the shear modulus, and ρ is the density (Mason, 1958). If we assume $\mu = K/2$, the calculated release velocity is 9.46 km/s and the minimum thickness of the impacting bodies is ~150 m. Because the shock durations in L-chondrites may be much longer than 40 ms, the impacting bodies are likely to be much larger. Using the 0.5 s shock-duration estimate from the survival of akimotoite, the body thickness would be 2 km.

5. Conclusions

Two unique high-pressure minerals are reported in Tenham, vitrified silicate-perovskite and akimotoite. Vitrified silicate-perovskite and akimotoite represent the products of crystallization from silicate melt at high pressure, which is different from the previously reported silicate-perovskite and akimotoite in Tenham which formed by solid-state transformation (Tomioka and Fujino, 1997), but the same as that in Acfer 040 (Sharp et al., 1997).

The mineralogy and micro-texture of the melt-vein matrix at the vein edge differ from those at the vein interior. The 520-μm-wide vein interior crystallized an assemblage of majorite plus magnesiowüstite, whereas the 30-μm-wide vein edge contains vitrified silicate-perovskite + akimotoite + ringwoodite + majorite. However, both mineral assemblages are consistent with crystallization from similar

pressure conditions: the melt-vein edge crystallized at 23–25 GPa and the vein interior crystallized at about 21–25 GPa. This relatively narrow pressure range suggests that the melt vein either crystallized at a constant equilibrium shock pressure of ~25 GPa or during slow release at a depth km below the surface of a parent body. This limited crystallization pressure range is not consistent with crystallization during rapid decompression from pressures >50 GPa.

Based on thermal modeling, the crystallization of the 580-μm-wide vein at ~25 GPa occurred over a time period of at least 40 ms corresponding to a shock pulse that was at least that long and probably much longer. Based on simple one-dimensional planar impact model, the shock calculation suggests that Tenham parent body experienced a shock with collision velocity ~2 km/s and a projectile size greater than 150 m in thickness.

Acknowledgments

We thank Carlton Moore and the Center for Meteorite Studies at Arizona State University for supplying the sample. We also thank John Wheatley, Karl Weiss, and Zhengquan Liu, and the Center for High Resolution Microscopy at ASU for assistance with the electron microscopy. We also thank Jim Clark for assistance with the electron microprobe. We thank W.U. Reimold, H.Leroux, A.El Goresy, and anonymous reviewer for helpful and critical reviews. We acknowledge NASA Cosmochemistry Grants NAG5-7285, NAG5-9381, and NAG5-1977 for supporting this research.

Associate editor: W. Uwe Reimold

References

Agee, C.B., Li, J., Shannon, M.C., Circone, S., 1995. Pressure-temperature phase diagram for the Allende meteorite. *J. Geophys. Res.* **100**, 725–740.

Ahrens, T.J., Johnson, M.L., 1995a. Shock wave data for minerals. In: Ahrens, T.J. (Ed.), *Mineral Physics & Crystallography: A handbook of physical constants*. American Geophysical Union.

Ahrens, T.J., Johnson, M.L., 1995b. Shock wave data for minerals. In: Ahrens, T.J. (Ed.), *Rock Physics and Phase relations: A handbook of physical constants*. American Geophysical Union.

Aramovich, C. J., Sharp, T. G., Wolf, G. 2003. The distribution and significance of shock-induced high-pressure minerals in chondrite skip wilson. *Lunar Planet. Sci.* XXXIV, 1355.pdf (abstr.).

Baer, M.R., 2000. Computational modeling of heterogeneous materials at the mesoscale. In: Furnish, M.D., Chabildas, L.C., Hixon, R.S. (Eds.), *CP505, Shock Compression of Condensed Matter-1999*. American Institute of Physics, pp. 27–33.

Beck, P., Gillet, P., El Goresy, A., Mostefaoui, S., 2005. Timescales of shock processes in chondritic and martian meteorites. *Nature* **435**, 1071–1074.

Bennett III, M.E., McSween, H.Y.J., 1996. Shock features in iron-nickel metal and troilite of L-group ordinary chondrites. *Meteoritics Planet. Sci.* **31**, 255–264.

Binns, R.A., 1970. $(Mg, Fe)_2SiO_4$ spinel in a meteorite. *Phys. Earth Planet. In.* **3**, 156–160.

Binns, R.A., Davis, R.J., Reed, S.J.B., 1969. Ringwoodite, natural $(Mg, Fe)_2SiO_4$ spinel in the Tenham meteorite. *Nature* **221**, 943–944.

Bischoff, A., Stöffler, D., 1992. Shock metamorphism as a fundamental process in the evolution of planetary bodies: Information from meteorites. *Eur. J. Mineral.* **4**, 707–755.

Bottke, J.W.F., Nolan, M.C., Greenberg, R., Kolvoord, R.A., 1994. Velocity distributions among colliding asteroids. *Icarus* **107**, 255–268.

Chen, M., Sharp, T.G., El Goresy, A., Wopenka, B., Xie, X., 1996. The majorite-pyrope + magnesiowüstite assemblage: constraints on the history of shock veins in chondrites. *Science* **271**, 1570–1573.

Chen, M., El Goresy, A., Frost, D., Gillet, P., 2004a. Melting experiments of a chondritic meteorite between 16 and 25 GPa: implication for Na/K fractionation in a primitive chondritic Earth's mantle. *Eur. J. Mineral.* **16**, 203–211.

Chen, M., Xie, X., El Goresy, A., 2004b. A shock-produced $(Mg, Fe)SiO_3$ glass in the Suizhou meteorite. *Meteoritics Planet. Sci.* **39**, 1797–1808.

Christiansen, E.H., Hamblin, W.K., 1995. *Exploring the planets*. Prentice-Hall, Englewoods Cliffs, NJ, 500p.

Cliff, G., Lorimer, G.W., 1975. The quantitative analysis of thin specimens. *J. Microsc.* **103**, 203–207.

DeCarli, P. S., 1979. Nucleation and growth of diamond in shock wave experiments: In K.D. Timmerhaus, M.S. Barber (Eds.), *High Pressure Science and Technology*, vol. 1, Plenum: New York, pp. 940–943.

DeCarli, P., Aramovich Weaver, C., Xie, Z., Sharp, T.G., 2004. Meteorite studies illuminate phase transition behavior of minerals under shock compression. In: Furnish, M.D., Gupta, Y.M., Forbes, J.W. (Eds.), *CP706, Shock Compression of Condensed Matter-200*. American Institute of Physics, pp. 1427–1430.

DeCarli, P.S., Bowden, E., Sharp, T.G., Jones, A.P., Price, G.D., 2002a. Evidence for kinetic effects on shock wave propagation in tectosilicates. In: Furnish, M.D., Thadhani, N.N., Horie, Y. (Eds.), *Shock Compression of Condensed Matter-2001*. American Institute of Physics, pp. 1381–1384.

DeCarli, P.S., Bowden, E, Jones, A.P., Price, G.D.,2002b. Laboratory impact experiments versus natural impact events. In: C. Koeberl, K.G. MacLeod (Eds.),*Catastrophic Events and Mass Extinctions: Impacts and Beyond, Boulder*. Geological Society of America Special Paper, Colorado, pp. 595–605.

Fei, Y., Bertka, C.M., 1999. Phase transitions in the Earth's mantle and mantle mineralogy. In: Fei, Y., Bertka, C.M., Mysen, B.O. (Eds.), *Mantle Petrology: Field Observations and High Pressure Experimentation: A Tribute to Francis R. (Joe) Boyd*. The Geochemical Society, pp. 189–207.

Fredriksson, K., DeCarli, P.S., Aaramäe, A., 1963. Shock-induced veins in chondrites. In: *Space Research III, Proceedings of the Third International Space Science Symposium*. North-Holland, pp. 974–983.

Gasparik, T., 1992. Melting experiments on the enstatite-pyrope join at 80–152 kbar. *J. Geophys. Res.* **97**, 15181–15188.

Gillet, P., Chen, M., Dubrovinsky, L., El Goresy, A., 2000. Natural $NaAlSi_3O_8$-hollandite in the shocked Sixiangkou meteorite. *Science* **287**, 1633–1636.

Irifune, T., 1993. Phase transformations in the earth's mantle and subducting slabs: Implication for their compositions, seismic velocity and density structures and dynamics. *Island Arc* **2**, 55–71.

Ito, E., Yamadah, H., 1982. Stability relations of silicate spinel, ilmenites and perovskites. In: Akimoto, S., Manghnani, M.H. (Eds.), *High-Pressure Research in Geophysics*. Center for Academic Publishing of Japan, pp. 405–419.

Ito, E., Navrotsky, A., 1985. $MgSiO_3$ ilmenite: calorimetry, phase equilibria, and decomposition at atmospheric pressure. *Am. Mineral.* **70**, 1020–1026.

Katsura, R., Ito, E., 1989. The system Mg_2SiO_4–Fe_2SiO_4 at high pressures and temperatures. Precise determination of stabilities of olivine, modified spinel and spinel. *J. Geophys. Res.* **94**, 15663–15670.

Kerschhofer, L., Sharp, T.G., Rubie, D.C., 1996. Intracrystalline transformation of olivine to wadsleyite and ringwoodite under subduction zone conditions. *Science* **274**, 79–81.

Kieffer, S.W., 1971. Shock metamorphism of the Coconino sandstone at Meteor Crater, Arizona. *J. Geophys. Res.* **76**, 5449–5473.

Kieffer, S.W., Phakey, P.P., Christie, J.M., 1976. Shock processes in porous quartzite: Transmission Electron Microscope observations and theory. *Contrib. Mineral. Petrol.* **59**, 41–93.

Klein, S.A., Beckman, W.A., Myers, G.E., 2002. FEHT: A Finite Element AnalysisProgram. F-Chart Software, http://www.fchart.com/download/feht.pdf.

Langenhorst, F., Joreau, P., Doukhan, J.C., 1995. Thermal and shock metamorphism of the Tenham chondrite: a TEM examination. *Geochim. Cosmochim. Acta* **59**, 1835–1845.

Langenhorst, F., Poirier, J.P., 2000. Anatomy of black veins in Zagami: clues to the formation of high-pressure phase. *Earth Planet. Sci. Lett.* **184**, 37–55.

Leroux, H., Doukhan, J.-C., Guyot, F., 2000. Metal-silicate interaction in quenched shock-induced melt of the Tenham L6-chondrite. *Earth Planet. Sci. Lett.* **179**, 477–787.

Madon, M., Poirier, J.P., 1983. Transmission electron microscope observation of α, β, γ $(Mg,Fe)_2SiO_4$ in shocked meteorites: planar defects and polymorphic transitions. *Phys. Earth Planet. In.* **33**, 31–44.

Mason, W.P., 1958. *Physical Acoustics and the Properties of Solids*. D. van Nostrand Company Inc, Princeton, NJ, 14p.

Mori, H., Takeda, H., 1985. Magnesiowüstite in a shock-produced vein of the Tenham chondrite. *Lunar Planet. Sci.* **XVI**, 579–598 (abstr).

Nesterenko, V.F., 2001. *Dynamics of Heterogeneous Materials*. Springer-Verlag, New York, 510p.

Price, G.D., Putnis, A., Agrell, S.O., 1979. Electron petrography of shock-produced veins in the Tenham chondrite. *Contrib. Mineral. Petrol.* **71**, 211–218.

Putnis, A., Price, G.D., 1979. High-pressure $(Mg,Fe)_2SiO_4$ phases in the Tenham chondritic meteorite. *Nature* **280**, 217–218.

Ringwood, A.E., 1958. The constitution of the mantle-II Further data on the olivine-spinel transition. *Geochim. Cosmochim. Acta* **15**, 18–29.

Sharp, T.G., DeCarli, P.S., 2006. Shock Effects in Meteorites. In: D.S. Lauretta, H.Y. McSween Jr. (Eds.), *Meteorites and the Early Solar System II.* University of Arizona Press (in press).

Sharp, T.G., Lingemann, C.M., Dupas, C., Stöffler, D., 1997. Natural occurrence of $MgSiO_3$-ilmenite and evidence for $MgSiO_3$-perovskite in a shocked L chondrite. *Science* **277**, 352–355.

Sharp, T. G., El Goresy, A., Chen, M., 2000. Nanocrystalline maskelynite in the Sixankou and Tenham L-6 chondrites: Microstructures of shocked plagioclase with the hollandite-structure. *Lunar Planet. Sci.* **XXXI**, 2085.pdf (abstr.).

Sharp, T. G., Xie, Z., Tomioka, N., 2001. Shock-induced melt veins in chondrites: crystallization history vs. shock history. *Lunar Planet. Sci.* **XXXII**, 2159.pdf (abstr.).

Sharp, T.G., Xie, Z., Aramovich, C.J., DeCarli, P.S., 2002. Pressure-temperature history of shock veins: A progress report. *Meteoritics Planet. Sci.* **37** (Suppl.), A129.

Sharp, T.G., Xie, Z., Aramovich, C.J., DeCarli P.S., 2003. Pressure-temperature histories of shock -induces melt veins in chondrites. *Lunar Planet. Sci.* **XXXIV**, 1278.pdf (abstr.).

Spencer, L.J., 1937. The Tenham meteoritic shower. *Mineral. Mag.* **24**, 437–452.

Stöffler, D., Keil, K., Scott, E.R.D., 1991. Shock metamorphism of ordinary chondrites. *Geochim. Cosmochim. Acta* **55**, 3845–3867.

Tomioka, N., Fujino, K., 1997. Natural $(Mg,Fe)SiO_3$-ilmenite and -perovskite in the Tenham meteorite. *Science* **277**, 1084–1086.

Tomioka, N., Mori, H., Fujino, K., 2000. Shock-induced transition of $NaAlSi_3O_8$ feldspar into a hollandite structure in a L6 chondrite. *Geophys. Res. Lett.* **27**, 3997–4000.

Trønnes, R.G., 2000. Melting relations and major element partitioning in an oxidized bulk Earth model composition at 15-26 GPa. *Lithos* **53**, 233–245.

van Cappellen, E., 1990. The parameterless correction method in X-ray microanalysis. *Microsc. Microanal. Microst.* **1**, 1–22.

van der Berg, A.P., Yuen, D.A., Steinbach, V., 2001. The effects of variable thermal conductivity on mantle heat transfer. *J. Geophys. Res.* **28**, 875–878.

Walsh, J.M., Christian, R.H., 1955. Equation of state of metals from shock wave experiments. *Phys. Rev.* **97**, 1544–1556.

Xie, Z., Sharp, T.G., 2000. Mineralogy of shock-induced melt veins in chondrites as a function of shock grade. *Lunar Planet. Sci.* **XXXI**, 2065.pdf (abstr.).

Xie, Z., Sharp, T.G., 2004. High-pressure phases in shock-induced melt veins of the Umbarger L6 chondrite: Constraints on shock pressure. *Meteoritics Planet. Sci.* **39** (12), 2043–2054.

Xie, Z., Tomioka, N., Sharp, T.G., 2001. High-pressure phases in shock-induced melt veins from the Umbarger L6 chondrite: Constrains on shock conditions. *Lunar Planet. Sci.* **XXXII**, 1805.pdf (abstr.).

Xie, Z., Tomioka, N., Sharp, T.G., 2002. Natural occurrence of Fe_2SiO_4-spinel in the shocked Umbarger L6 chondrite. *Am. Mineral.* **87**, 1257–1260.

Zener, C., Hollomon, J.H., 1944. Effect of strain rate on plastic flow of steel. *J. Appl. Phys.* **15**, 22–32.

Zhang, J., Herzberg, C., 1994. Melting experiments on anhydrous peridotite KLB-1 from 5.0 to 22.5 GPa. *J. Geophys. Res.* **99**, 17729–17742.